Available online at www.sciencedirect.com
SCIENCE DIRECT®
Catalysis Today 89 (2004) 325–330
CATALYSIS TODAY
www.elsevier.com/locate/cattod

Magnetic anisotropy and microstructure in sputtered CoPt(1 1 0) films

M. Abes [a,*], O. Ersen [a], E. Elkaïm [b], G. Schmerber [a], C. Ulhaq-Bouillet [a], A. Dinia [a], P. Panissod [a], V. Pierron-Bohnes [a]

[a] *Institut de Physique et de Chimie des Matériaux de Strasbourg (UMR 7504 du CNRS), ULP-ECPM-CNRS, BP 43, 23 Rue du Loess, 67034 Strasbourg Cedex 2, France*
[b] *Laboratoire pour l'Utilisation du Rayonnement Electromagnétique (LURE), Centre Universitaire, Bât. 209D, BP 34, 91898 Orsay Cedex, France*

Abstract

We compare structural and magnetic properties of CoPt films sputtered at 900 K on MgO(1 1 0) (with a Pt(1 1 0) buffer layer) and MgO(0 0 1) (with a Pt(0 0 1) buffer layer) substrates. We obtain a layer with the $L1_0$ tetragonal structure. The equiatomic $L1_0$ phase is a "natural" multilayer, which consists in a stacking along the [0 0 1] direction of pure Co and pure Pt monolayers. At this temperature, the growth of CoPt yields nearly single orientation epitaxial films: CoPt(1 1 0)[0 0 1]//MgO(1 1 0)[0 0 1] and CoPt(0 0 1)[1 1 0]//MgO(0 0 1)[1 1 0] as shown by transmission electron microscopy. On MgO(1 1 0) substrates, the long-range chemical ordering is incomplete in contrast with the case of MgO(0 0 1) substrates, where long-range order is nearly perfect. Despite incomplete chemical ordering, a large in-plane magnetic anisotropy is present for the films grown on the MgO(1 1 0) substrate. This is interesting for the magnetic recording writing with a classical recording head and reading with a magnetoresistance head. The structural study of the CoPt films grown on MgO(1 1 0) has pointed out that three variants of the $L1_0$ phase coexist. The proportion of [1 0 0] and [0 1 0] variants, oriented at 45° with the ordering growth direction, is much higher than the proportion of the [0 0 1] variant. In fact, the simulation of magnetization loops has shown that the easy magnetization axis is within the plane along the [1,−1,0] direction. This anisotropy is favored for the [1 0 0] and [0 1 0] variants. On MgO(0 0 1), the CoPt films grow as a single variant with the concentration modulation and the magnetic anisotropy along the growth direction.

Keywords: Alloys; Chemical order; Magnetic anisotropy; Sputtering epitaxy

1. Introduction

The $L1_0$ ordered phase is an equilibrium phase in the CoPt bulk phase diagram [1,2] and is obtained from the fcc disordered state by annealing it below 1000 K. Its structure is based on a face centered cubic lattice with pure Co and Pt planes stacked along the [0 0 1] direction (*c*-axis), producing a tetragonal distortion along this direction. Long-range order may occur along the three equivalent [1 0 0], [0 1 0] and [0 0 1] crystallographic directions. In order to obtain a crystal ordered along a single direction it is necessary to anneal it in presence of an external stress (such as a magnetic field or a mechanical stress [3]).

We have shown earlier [4] that CoPt films, grown by sputtering on Pt(0 0 1)/MgO(0 0 1) substrates, order spontaneously during the growth at 900 K and have a long-range order (LRO) parameter (*S*) as high as 0.80. This $L1_0$ ordered phase exhibits a large perpendicular magnetic anisotropy as observed experimentally by Ersen et al. [5] or Grange et al. [6] and theoretically by others groups [7,8]. The easy axis is along the tetragonal *c*-axis, which is the ordering axis. The anisotropy energy K_u is predicted to reach a value as large as 10^6 J/m^3. This is one of the highest anisotropy energies predicted in transition metal alloys and results from the spin polarization of the Pt 5*d* band combined with the spin–orbit [6–9] coupling on Pt. These systems are particularly interesting for magneto-optic [10] recording because they exhibit large Kerr [11] effect signals and because they are chemically stable.

The aim of the present study is to compare this result with CoPt films grown under similar conditions with using another substrate orientation such as Pt/MgO(1 1 0). In this paper, we report the magnetic and microstructural characterization of sputtered CoPt(1 1 0) films deposited at 900 K onto Pt seed layers on MgO(1 1 0) substrates. We also discuss the influence of film orientation on its ordering.

* Corresponding author. Tel.: +33-388-10-70-77; fax: +33-388-10-72-49.
E-mail address: abes@ipcms.u-strasbg.fr (M. Abes).

0920-5861/$ – see front matter © 2003 Elsevier B.V. All rights reserved.
doi:10.1016/j.cattod.2003.12.008

2. Experimental procedures

The samples consist of a 50 nm thick epitaxial $Co_{50}Pt_{50}$ layer, grown on a 10 nm thick Pt seed film on a MgO substrate. Two orientations of the substrate have been used: (0 0 1) and (1 1 0). To prevent them from oxidation, all samples were covered by a 5 nm thick Pt capping layer at room temperature.

X-ray diffraction measurements were performed on a D-500 Siemens diffractometer equipped with a monochromatic Co $K\alpha_1$ incident beam ($\lambda = 0.17889$ nm). ω–2θ reflection scans and rocking curves in symmetrical and asymmetrical geometries were collected (ω is the incident angle). Using a home made sample holder with a rotation axis in the diffraction plane, we have optimized the diffracted intensity, versus the orientation of the sample around both axes in its plane.

Diffraction scans were also performed on the W22 instrument ($\lambda = 0.0698$ nm) of the Laboratoire pour l'Utilisation du Rayonnement Electromagnétique (LURE) in Orsay, France. The high-order diffraction peaks have been measured on a CoPt(1 1 0) sample deposited on the MgO(1 1 0) substrate to estimate the Debye–Waller attenuation factors and to obtain absolute values of the chemical LRO parameter.

Transmission electron microscopy (TEM) images and diffraction patterns were obtained both in plan view and in cross-section using a Topcon-002B microscope operating at 200 kV. The samples have been thinned first mechanically and then by ion milling.

3. Diffraction theory

The long-range order parameter (S) in a binary ordered alloy A_xB_{1-x} is defined from the difference between c_A^1 and c_A^2, the A atomic concentrations in the A-rich and A-poor planes, respectively:

$$S = \frac{c_A^1 - c_A^2}{2(1-x)} \tag{1}$$

For the pseudo-cubic cell, the structure factor has a different form for fundamental peaks ($h\,k\,l$ with the same parity):

$$F_F = 2(f_A + f_B)\,e^{-(M_F^T + M_F')} \tag{2a}$$

and for superstructure peaks ($h\,k\,l$ mixed):

$$F_S = 2S(f_B - f_A)\,e^{-(M_S^T + M_S')} \tag{2b}$$

where f_i is the atomic scattering factor of atom i, M_F^T, M_S^T represent the contributions of mean-square thermal vibrations ($\langle u_T^2 \rangle$) to the attenuation of Bragg peaks. M_F', M_S' represent the contributions due to mean-square static displacements from lattice sites. All M terms have the form: $B(\sin^2\theta/\lambda^2)$, where B is the Debye–Waller (D–W) attenuation factor. To get long-range order parameters from X-ray line intensities, we need an evaluation of the Debye–Waller attenuation factors at room temperature. They have been measured in a CoPt sample on W22 at LURE, using the method developed by Berg and Cohen [12].

The intensities of the observed peaks have been obtained by multiplying the integrated $\omega/2\theta$ curves by the width of the rocking curve. They have been corrected by the X-ray atomic diffusion and Lorentz-polarization irradiated area factors (LP). From the integrated intensities of fundamental (P_F) and superstructure (P_S) peaks, we get using Eq. (2):

$$\ln\left\{\frac{1}{2(f_A + f_B)}\left(\frac{P_F}{LP}\right)^{1/2}\right\} = \frac{1}{2}\ln K - (M_F^T + M_F') \tag{3a}$$

$$\ln\left\{\frac{1}{2S(f_B - f_A)}\left(\frac{P_S}{LP}\right)^{1/2}\right\} = \frac{1}{2}\ln K - (M_S^T + M_S') \tag{3b}$$

Straight lines are obtained when plotting the left-hand side of Eq. (3) versus $(\sin^2\theta/\lambda^2)$. The K term is a constant including the incident beam intensity. Knowing $(M_F^T + M_F')$ and $(M_S^T + M_S')$, the ratio of the integrated intensities of superstructure and fundamental peaks was then employed to obtain S

$$S_z = \left\{\left(\frac{P_S}{P_F}\frac{(LP)_F}{(LP)_S}\right)^{1/2}\frac{(f_A + f_B)\,e^{-(M_F^T + M_F')}}{(f_A - f_B)\,e^{-(M_S^T + M_S')}}\right\} \tag{4}$$

In the case of a multi-variant sample, as the fundamental peaks corresponding to the different variants could not be separated, the value obtained using (4) for a given variant is the product of the average long-range order within the grains of this variant and the proportion of this variant within the sample.

4. X-ray diffraction and microstructural analysis

X-ray diffraction (XRD) scans provide information on both structure and chemical order in the films. Fig. 1 shows $\theta/2\theta$ scans. Besides the MgO substrate (2 2 0) peak (not shown here), different diffraction peaks corresponding to the Pt buffer layer and to the CoPt alloy film are distinctly observed: the (2 2 0) fundamental peaks are present (Fig. 1), as well as the (1 1 0) superstructure line characteristic of the CoPt $L1_0$ ordered phase (inset in Fig. 1). This shows that the growth of Pt and CoPt is epitaxial on the MgO(1 1 0) substrate. Transmission electron microscopy experiments have confirmed that this is the only growth direction. These XRD measurements reveal an important mixing at the CoPt/Pt interface during the growth. This thickening of this interfacial layer can contribute to the decrease of the long-range order parameter, as perfect order can only be obtained in stoichiometric samples.

The $L1_0$ equilibrium phase can present three variants: the concentration modulation can occur along the [1 0 0] and

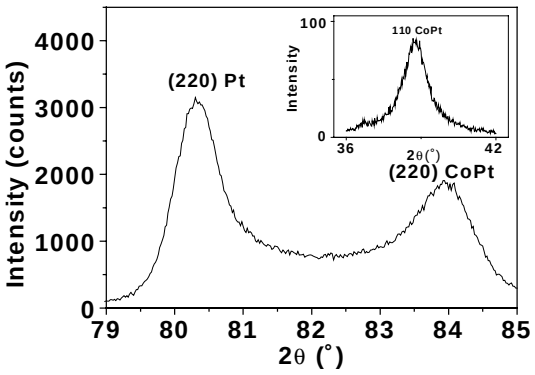

Fig. 1. θ–2θ scanned diagram around the (2 2 0) fundamental peak and the (1 1 0) superstructure (inset) peaks for co-sputtered CoPt alloy deposited on a MgO(1 1 0) substrate. The diagrams were recorded at room temperature using a monochromatic Co radiation ($\lambda_{K\alpha 1} = 0.17889$ nm).

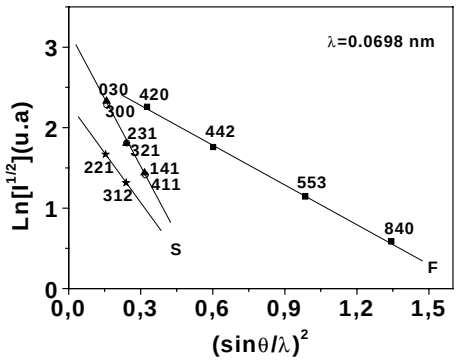

Fig. 3. $\ln(K^{1/2}\,e^{-M})$ vs. $\sin^2\theta/\lambda^2$, where $K^{1/2}\,e^{-M}$ is the square root of the integrated intensity divided by the Lorentz factor and F^2. S: superstructure peaks for the three variants; F: fundamental peaks, measurements have been done at $T = 300$ K.

[0 1 0] directions at 45° with respect to the growth direction, or in the [0 0 1] direction in the growth plane. The latter variant is at the origin of the (1 1 0) superstructure peak observed with the scattering vector along the surface normal. We measured the (1 2 0) and (2 1 0) peaks (Fig. 2), corresponding, respectively, to [1 0 0] and [0 1 0] variants. The slopes of the straight lines of Eq. (3) lead to $B_F = 0.0163\,nm^2$ for the fundamental peaks and to $B_x = 0.0542\,nm^2$, $B_y = 0.0565\,nm^2$, and $B_z = 0.0411\,nm^2$ for the different variants (Fig. 3).

As we could not separate the fundamental peaks of the different variants, the LRO parameter S was calculated using Eq. (4) with the sum of the integrated intensities of (1 1 0), (1 2 0), (2 1 0) peaks for P_S and the integrated intensity of (2 2 0) peak for P_F. For a perfectly ordered film, S is equal to 1 in this case too. We find an average order parameter $S = 0.48$. This shows that chemical order is lower than in the CoPt film [4] deposited on a MgO(0 0 1) substrate, where $S = 0.80$. The full width at half maximum (FWHM) of the (1 1 0) superstructure peak (1.2°) is larger than the FWHM of the (0 0 1) peak in the CoPt(0 0 1) film (0.4°) [4]. This indicates that the perpendicular coherence

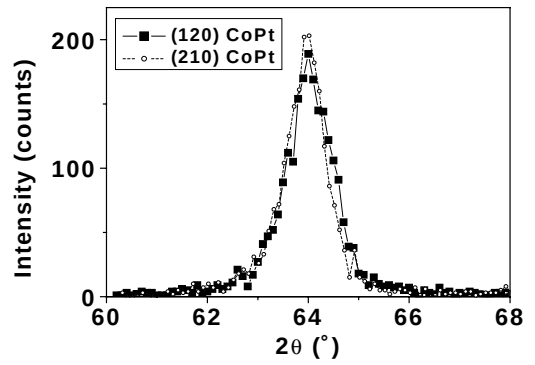

Fig. 2. ω–2θ scanned diagram around the (1 2 0) and (2 1 0) superstructure peaks for co-sputtered CoPt alloy deposited on a MgO(1 1 0) substrate corresponding, respectively, to the [1 0 0] and [0 1 0] variants of the $L1_0$ phase. The diagrams were recorded at room temperature using a monochromatic Co radiation ($\lambda_{K\alpha 1} = 0.17889$ nm).

length of the CoPt(0 0 1) film (20 nm) is higher than in the CoPt(1 1 0) film (7 nm). Information on the extent of the lattice order cannot be deduced from the (2 2 0) peak FWHM here, since the presence of different variants in the film leads to a peak splitting as a result of the different lattice constants. The a lattice parameter deduced from the position of the CoPt(1 1 0) reflection is $a = 0.38$ nm, whereas the value deduced from the CoPt(220) reflection is $a = 0.377$ nm due to the presence of the [1 0 0] and [0 1 0] variants.

On the other hand, the perpendicular mosaic spread for the CoPt(2 2 0) fundamental peak is smaller than 1.3° (FWHM of the rocking curve) indicating a good crystalline quality of the sample, even if worse than in the CoPt(0 0 1) film (0.8°).

Transmission electron microscopy was carried out on cross-section foils prepared from the sample grown on the MgO(1 1 0) substrate. Figs. 4 and 5 show high-resolution electron images as recorded along [0 0 1] and [1,−1,0] azimuths, respectively. High quality epitaxial growth of the CoPt is confirmed by lattice fringes observed in both the substrate and the CoPt in Fig. 4. Selected-area electron diffraction patterns (not shown here) also confirmed the epitaxial growth. Slight roughness of both MgO/Pt and Pt/CoPt interfaces, probably due to steps on MgO surface, is also evident in Fig. 4 but it does not noticeably disrupt epitaxy. There is no obvious evidence of the interdiffusion between the Pt seed film and the CoPt film during the growth.

This image also clearly shows regions with a doubling of the period of (2 0 0) and (0 2 0) fringes and other regions where this doubling is weaker or entirely absent. This period doubling is a signature of the CoPt $L1_0$ phase with the compositional modulation (c-axis) along [1 0 0] or [0 1 0] directions. For the [0 0 1] variant no modulation can be observed in the [0 0 1] azimuth. The inset of Fig. 4 shows the Fourier transform (or diffraction pattern) of the region where the double period is well contrasted: both (1 0 0) and (0 1 0) half-order satellite spots are clearly visible.

On the high-resolution electron image recorded along the [1,−1,0] azimuth, there is no region with a doubling of the period of the (0 0 2) fringes, which confirms that the

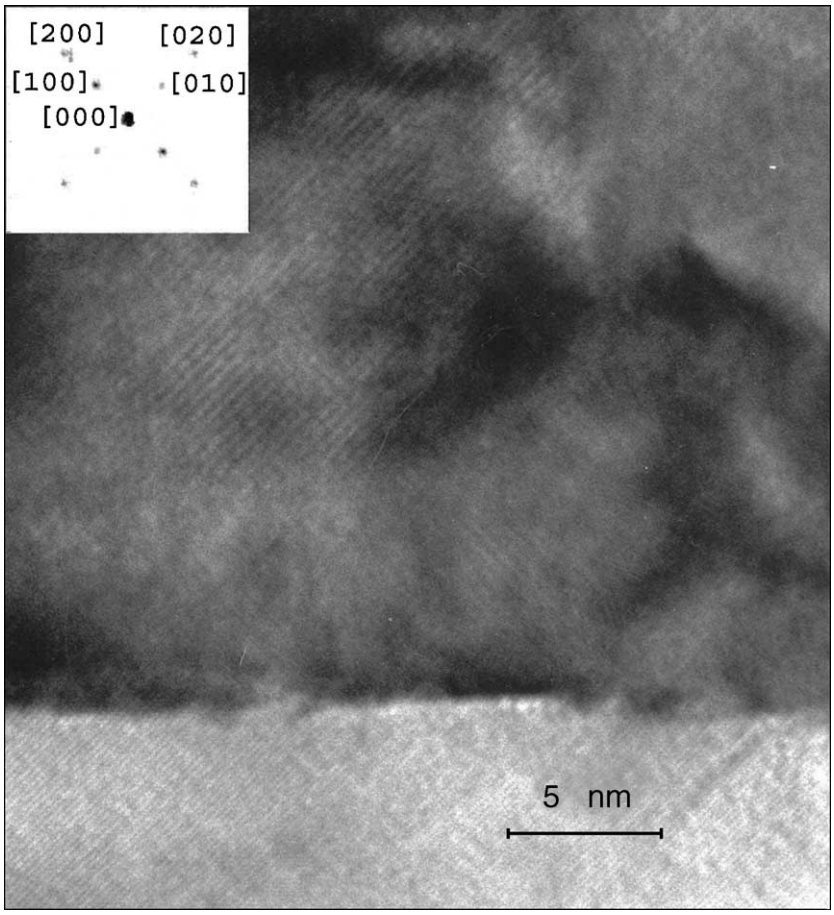

Fig. 4. Transmission electron micrograph showing cross-section of CoPt(1 1 0) sample. [0 0 1] projection showing CoPt/Pt/MgO interface region. Note the inhomogeneous distribution of the $L1_0$ phase indicated by regions with doubling of periodicity of (1 0 0) and (0 1 0) lattice fringes and computed diffraction pattern (inset) with $L1_0$ satellite spots.

proportion of [1 0 0] and [0 1 0] variants is much higher than the proportion of the [0 0 1] variant. We see that the (1 1 1) and (0 0 2) planes are visible as confirmed by the Fourier transform (inset in Fig. 5). In this direction, it is possible that we do not observe the doubling of the period of (0 0 2) fringes because the (1 1 1) planes are the most dense planes. The microscope resolution is highly sensitive to these planes.

5. Magnetic characterization

M–H loops (Fig. 6) for the two CoPt(1 1 0) samples were recorded using an alternating gradient field magnetometer (AGFM) to determine the saturation magnetization and the easy magnetization axes. The field was applied in-plane along the CoPt [0 0 1] and [1,−1,0] directions and along the normal plane of the film (CoPt [1 1 0]). Fig. 6 shows the loops for these three directions. The contribution of the diamagnetic susceptibility of the MgO substrate is evaluated from the magnetization curves set up with the external field parallel to the easy magnetization axis. The easiest axis is in the plane along the CoPt[1,−1,0] direction, and the saturation magnetization is $M_s = 770\,\text{emu/cm}^3$. The [0 0 1] direction is magnetically the hardest, as can be seen from incomplete saturation along this direction. The saturation is more difficult along the perpendicular direction to the film than in [1,−1,0] direction since the demagnetizing field has to be overcome.

The magnetization loops for the CoPt(0 0 1) ordered film (dotted line in Fig. 6) have a perpendicular easy magnetization axis. The total anisotropy energy or the effective anisotropy (K_{eff}) of the film can be written as follows:

$$K_{\text{eff}} = K_u - 2\pi M_s^2$$

where $2\pi M_s^2$ is the macroscopic shape anisotropy term, and K_u the uniaxial anisotropy energy. These anisotropy terms [4] have been determined for this ordered film and correspond, respectively, to 0.29×10^6 and $3.2 \times 10^6\,\text{J/m}^3$. This shows that the contribution of the shape anisotropy energy is much smaller than the uniaxial anisotropy. On the contrary, the magnetocrystalline anisotropy parameters for the CoPt(1 1 0) film reported in Fig. 6 are weaker. Indeed, as shown in this figure the shape anisotropy is high enough to make the saturation of the magnetization harder along the [1 1 0] direction. This means that this term is of the same order than the magnetocrystalline anisotropy for the [1 0 0]

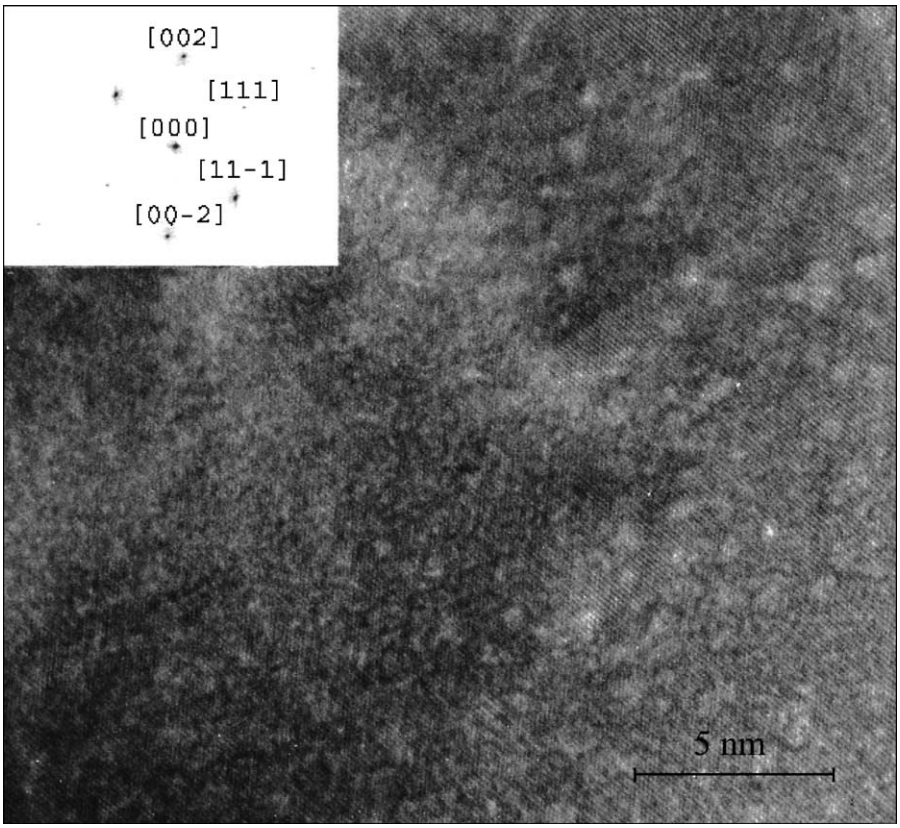

Fig. 5. Transmission electron micrograph showing cross-section of CoPt(1 1 0) sample with computed diffraction pattern (inset); direction [1,−1,0].

and [0 1 0] variants, which is in this case much smaller than that for the CoPt(0 0 1) ordered film. To further support the previous analysis, we have simulated magnetization loops with the following parameters: the same values for demagnetizing and magnetocrystalline anisotropy fields $H_d = H_a = 1$ T, while the saturation magnetization was fixed at $M_s = 800$ emu/cm^3 and a negligible coupling between grains of the three different variants (three different easy magnetization axes). The results of this simulation are reported in Fig. 7 and agree qualitatively with the experimental loops

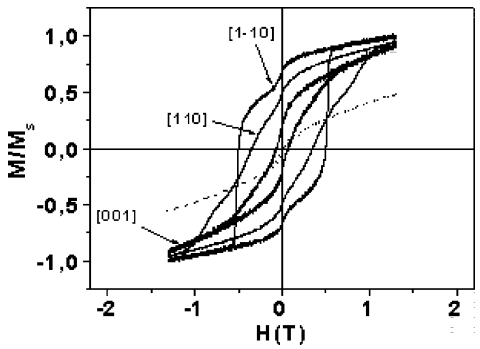

Fig. 6. Normalized magnetization loops measured by AGFM at 300 K for the CoPt(1 1 0) and CoPt(0 0 1) films. Field applied in-plane along easy axis: CoPt[1,−1,0], in-plane along CoPt[0 0 1] and along the normal plane of the film: CoPt[1 1 0] for the CoPt(1 1 0) film (full lines). Field applied in-plane along hard axis for the CoPt(0 0 1) film (dotted line).

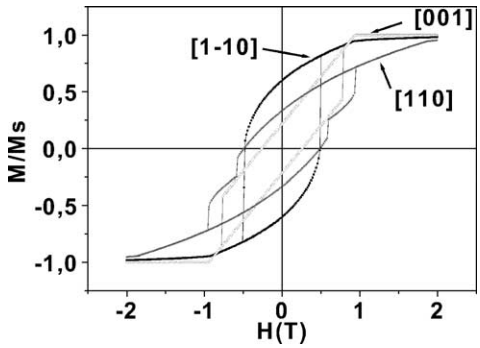

Fig. 7. Simulation of magnetization loops with parameters: $H_d = 1$ T, $H_a = 1$ T and a negligible K coupling between grains. Field applied in-plane along the easy axis: [1,−1,0], in-plane along the [0 0 1] direction and along film normal [1 1 0].

(Fig. 6). They confirm that the magnetization is the easiest along the [1,−1,0] direction as expected for a majority of [1 0 0] and [0 1 0] variant grains.

6. Discussion and conclusions

We have found that the state of chemical order is relatively inhomogeneous in the CoPt(1 1 0) films grown at 900 K. The long-range order (0.48 in average) is significantly smaller than in CoPt(0 0 1) oriented films grown

under similar conditions (0.80) and three variants to the $L1_0$ phase are present. The results of X-ray diffraction and magnetization loop measurements show that the proportion of [1 0 0] and [0 1 0] variants is much higher than the proportion of [0 0 1] variant. Despite their lower magnetic and structural anisotropy, the CoPt(1 1 0) films present a large in-plane magnetocrystalline anisotropy with the easiest magnetization axis along [1,−1,0].

For the equiatomic CoPt alloy films codeposited by molecular-beam epitaxy (MBE [13]) or by sputtering [4] on MgO(0 0 1) substrates, the ordering occurs mainly along the [0 0 1] crystallographic direction. This can be related to two different effects: (i) the influence of the buffer layer and (ii) the Pt segregation at the growth surface [14,15]. For a growth temperature of 900 K (below the order–disorder transition (1100 K), but high enough to allow atomic mobility), we expect of course the formation of the tetragonal $L1_0$ phase. The influence of the Pt buffer layer can be regarded as an external stress for the growth: the lattice parameter of Pt is 0.392 nm, much larger than the *c* parameter of the $L1_0$ phase (0.369 nm), and closer to the *a* parameter of $L1_0$ phase (0.381 nm). There is, therefore, a tendency for the tetragonalization along the [0 0 1] growth direction. Moreover, the occurrence of a bilayer by bilayer growth can also be greatly enhanced by the Pt segregation on the advancing surface during growth allowed by surface diffusion. This effect also can lead to the formation of an alternation of Pt-rich and Pt-poor planes perpendicular to the growth direction. Finally, these two combined effects yield the formation of an almost perfect superlattice constituted of alternating Co and Pt planes perpendicular to the growth direction.

For the CoPt alloy films deposited on the MgO(1 1 0) substrates, the orientation of the *c*-axis is different: the three variants of the $L1_0$ phase coexist. The proportion of [1 0 0] and [0 1 0] variants, with the ordering direction oriented at 45° from the growth direction, is much higher than the proportion of the [0 0 1] variant. Following the same approach as before to understand the origin of this microstructure, we can expect the following tendencies: the stress effect is smaller in this case than in the [0 0 1] growth direction: in the (1 1 0) plane, the epitaxial cell is based on the 1, −1, 0 and 0 0 1 vectors. Its surface $a(a^2 + c^2)^{1/2}$ for the [1 0 0] and [0 1 0] variants and $2^{1/2}ac$ for the [0 0 1] variant. The epitaxial stress on a larger substrate is therefore smaller for the [1 0 0] and [0 1 0] variants. On the other hand, the segregation effect on the growth surface (1 1 0) has the tendency to favor the [0 0 1] variant that presents an alternation of pure planes along the [1 1 0] direction. Moreover, the Pt(1 1 0)/MgO(1 1 0) surface are known to present in some case [16] a reconstruction with factory roofs, faceting along {1 0 0} type planes. This faceting, combined with the easy growth with *c*-axis along the growth direction on these facets, would explain the domination of the [1 0 0] and [0 1 0] variants.

These two variants have individually an easy axis along [1 0 0] and [0 1 0], respectively. Their combination with the geometrical demagnetizing field that orients the magnetization in the plane explains the easy magnetization axis in the [1,−1,0] direction that we observe. This average magnetization is in fact the composition of two different magnetizations: along the [1 0 0] and [0, −1, 0] for the grains of the two dominant variants, as well described by the simple model presented. For technological reasons, a great interest has been shown recently in films exhibiting in-plane magnetic anisotropy for their application as magnetic recording media [17].

References

[1] T.B. Massalski, Binary Alloy Phase Diagrams, 2nd ed., ASM International, USA, 1990.
[2] C.E. Dahmani, M.C. Cadeville, V. Pierron-Bohnes, Acta Metall. 33 (1985) 369.
[3] K. Morioka, K. Tanaka, in: S. Hanada, Z. Zhong, S.W. Nam, R.N. Wright (Eds.), Proceedings of the Fourth Rim International Conference on Advanced Materials and Processing (PRICM4), 2001, p. 1703.
[4] M. Abes, O. Ersen, D. Muller, M. Acosta, C. Ulhaq-Bouillet, A. Dinia, V. Pierron-Bohnes, Mater. Sci. Eng. C 23 (2003) 229.
[5] O. Ersen, V. Parasote, V. Pierron-Bohnes, M.C. Cadeville, C. Ulhaq-Bouilllet, J. Appl. Phys. 93 (2003) 2987.
[6] W. Grange, I. Galanakis, M. Alouani, M. Maret, J.-P. Kappler, A. Rogalev, Phys. Rev. B 62 (2000) 1157.
[7] I. Galanakis, M. Alouani, H. Dreyssé, Phys. Rev. B 62 (2000) 6475.
[8] S.A. Razee, J.P. Staunton, B. Ginatempo, F.J. Pinski, E. Bruno, Phys. Rev. Lett. 82 (1999) 5369.
[9] P. Bruno, Phys. Rev. B 39 (1989) 865.
[10] L. Uba, S. Uba, V.N. Antonov, A.N. Yaresko, R. Gontarz, Phys. Rev. B 64 (2001) 125105.
[11] E. Beaurepaire, M. Maret, V. Halté, J.C. Merle, A. Daunois, J.-Y. Bigot, Phys. Rev. B 58 (1998) 12134.
[12] H. Berg, B.J. Cohen, Metall. Trans. 3 (1972) 1797.
[13] V. Parasote, M.C. Cadeville, G. Garreau, E. Beaurepaire, J. Magn. Magn. Mater. 198–199 (1999) 375.
[14] Y. Gauthier, R. Baudoing-Savois, J.M. Bugnard, U. Bardi, A. Atrei, Surf. Sci. 276 (1992) 1.
[15] S. Ferrer, P. Fajardo, F. de Bergevin, J. Alvarez, X. Torrelles, H.A. Van Der Vegt, H. Etgens, Phys. Rev. Lett. 77 (1996) 747.
[16] S. Dubourg, J.-F. Bobo, B. Warot, E. Snoeck, J.-C. Ousset, Phys. Rev. B 64 (2001) 54416.
[17] K.R. Coffey, M.A. Parker, J.K. Howard, IEEE Trans. Magn. 31 (1995) 2737.